PHYSICAL REVIEW D **95,** 034040 (2017)

Relativistic effects in model calculations of double parton distribution functions

Matteo Rinaldi[1] and Federico Alberto Ceccopieri[2,3]

[1]*Instituto de Fisica Corpuscular (CSIC-Universitat de Valencia), Parc Cientific UV, c/Catedratico Jose Beltran 2, E-46980 Paterna, Valencia, Spain*

[2]*Dipartimento di Fisica e Geologia, Università degli Studi di Perugia and Istituto Nazionale di Fisica Nucleare, Sezione di Perugia, via A. Pascoli, I-06123 Perugia, Italy*

[3]*IFPA, Université de Liège, B4000 Lìege, Belgium*

(Received 19 November 2016; published 28 February 2017)

In this paper we consider double-parton distribution functions (dPDFs), which are the main nonperturbative ingredients appearing in the double-parton scattering cross section formula in hadronic collisions. By using recent calculation of dPDFs by means of constituent quark models within the so-called light-front approach, we investigate the role of relativistic effects on dPDFs. We find, in particular, that the so-called Melosh operators, which allow us to properly convert the LF spin into the canonical one and incorporate a proper treatment of boosts, produce sizeable effects on dPDFs. We discuss specific partonic correlations induced by these operators in the transverse plane which are relevant to the proton structure, and we study under which conditions these results are stable against variations in the choice of the proton wave function.

DOI: 10.1103/PhysRevD.95.034040

I. INTRODUCTION

A proper description of final states in hadronic collisions requires the inclusion of multiple-partonic interactions (MPIs) [1–3]—i.e., a mechanism which takes into account the possibility that more than one pair of partons may interact in a given hadronic collision. This possibility emerges naturally, since both colliding hadrons are extended objects in the transverse plane, at variance with processes involving pointlike probes, as in deep inelastic scattering where, to date, no MPI effects have been reported. Multiple-parton interactions enhance particle yields at low transverse momenta, affecting multiplicities and energy flows. MPIs play an important role also in events characterized by a hard scale, where they may contaminate the primary event with the production of secondaries which contribute to the so-called underlying event. In recent years, given the LHC operation, renewed interest has been paid to double-parton scattering (DPS), in which a couple of partons from each hadron interact with each other. If both interactions are hard enough, perturbative techniques can be applied and, as such, this class of processes need to be well controlled, since they might represent a background to New Physics searches. At the same time, DPS has its own physical interest, being sensitive to the nucleon structure. In particular, the cross section for this process depends on nonperturbative quantities, the so-called double-parton distribution functions (dPDFs). The latter encode the probability of finding two interacting partons, with a longitudinal momentum fraction with respect to the proton one, x, and the relative transverse distance $\vec{b}_\perp$, offering the opportunity to investigate parton momentum and spin correlations in the nucleon, unveiling new information on its structure; see Ref. [4]. Since dPDFs are two-body distributions, this knowledge is complementary to that encoded in other types of (one-body) distributions, such as generalized parton distributions (GPDs) and transverse-momentum-dependent distributions (TMDs). To date, dPDFs are very poorly known objects. Little guidance on their structure comes from sum rules, which relate them to ordinary PDFs—see Refs. [5,6]—while their perturbative QCD evolution is still debated due to the presence of the so-called inhomogeneous term in the evolution equations—see Refs. [7–10]. In this situation, it is clear that a proper theoretical modelization of a DPS signal is quite challenging. This problem has been circumvented phenomenologically by expressing the DPS cross section $\sigma_{\rm DPS}$ with the final state $A+B$ by the following ratio; see e.g. Ref. [11]:

$$\sigma_{\rm DPS}^{A+B} = \frac{m}{2}\frac{\sigma_{SPS}^{A}\sigma_{SPS}^{B}}{\sigma_{\rm eff}}, \tag{1}$$

where m is a combinatorial factor depending on the final states A and B ($m=1$ for $A=B$ or $m=2$ for $A\neq B$), and $\sigma_{SPS}^{A(B)}$ is the single-parton scattering cross section with the final state $A(B)$. Expressing the $\sigma_{\rm DPS}$ cross section in Eq. (1) in terms of the product of σ_{SPS}, one assumes that as a first approximation, the two hard scatterings can be factorized, and that double-parton distributions can be written as

$$F_{ab}(x_1,x_2,b_\perp,Q^2) \sim f_a(x_1,Q^2) f_b(x_2,Q^2) T(b_\perp), \tag{2}$$

where $f_a(x_1, Q^2)$ and $f_b(x_2, Q^2)$ are the standard PDFs evaluated at the scale Q^2. The function $T(b_\perp)$ captures parton correlations in the transverse plane. This ansatz for dPDFs exploits the idea that, for decreasing parton fractional momenta x, the parton population in the nucleon increases, resulting in a substantial longitudinal decorrelation of the joint distribution F_{ab}. The double-parton interaction rate is then totally encapsulated in the function $T(b_\perp)$. In such a factorized approach, the effective cross section appearing in Eq. (1) is simply given by

$$\sigma_{\rm eff}^{-1} = \int d^2b_\perp [T(b_\perp)]^2 \tag{3}$$

and, by construction, does not show any dependence on parton fractional momenta, hard scales, or parton species. Due to the rather easy technical implementation of Eq. (1) and the almost total inclusiveness of the experimental analyses performed so far, all the present knowledge on DPS cross sections has been condensed in the experimental and model-dependent extraction of $\sigma_{\rm eff}$ [11–18]. To date, the corresponding number determined so far ($\sigma_{\rm eff} \simeq 15$ mb) is compatible, within errors, with a constant, irrespective of the center-of-mass energy of the hadronic collisions and final state $(A + B)$ considered. Given this situation, many features of dPDFs are essentially unconstrained. It is therefore clear that nonperturbative methods may give access to some relevant properties on these distributions [19–24], allowing us, for example, to establish to what extent such dPDFs models may correctly reproduce the magnitude of the transverse correlation encoded in $\sigma_{\rm eff}$; see, for instance, the results of Refs. [25,26] on this point.

In this work, starting from the results obtained in Ref. [21], where dPDFs have been calculated in the valence region within a fully relativistic covariant treatment, the so-called light-front (LF) approach, we identify model-independent effects induced on dPDFs by the relativistic treatment—in particular, the violation of the factorized ansatz and the effects of parton correlation in the transverse plane in the proton structure. We also try to quantify the corresponding impact on observable-related quantities.

The paper is organized as follows: In Sec. II, we outline the structure of dPDFs and relativistic operators. In Sec. III, we describe the details of the hadronic models used in the analysis. In Sec. IV, we discuss the relevant issue of dPDF factorization in longitudinal and transverse space and the impact of the correct treatment of relativistic effects on dPDFs. We finally draw our conclusions in Sec. V.

II. THE LIGHT-FRONT APPROACH AND RELATIVISTIC EFFECTS

Following Ref. [21], dPDFs have been calculated starting from their light-cone correlator, which formally defines them in QCD. A suitable expression for dPDFs has been presented in Ref. [21]:

$$\begin{aligned} F(x_1, x_2, \vec{k}_\perp) \propto & \int d\vec{k}_1 d\vec{k}_2 \Psi\left(\vec{k}_1 + \frac{\vec{k}_\perp}{2}, \vec{k}_2 - \frac{\vec{k}_\perp}{2}\right) \\ & \times \Psi^\dagger\left(\vec{k}_1 - \frac{\vec{k}_\perp}{2}, \vec{k}_2 + \frac{\vec{k}_\perp}{2}\right) \\ & \times \delta\left(x_1 - \frac{k_1^+}{M_0}\right)\delta\left(x_1 - \frac{k_1^+}{M_0}\right) \\ & \times \langle SU(6)|D_1^\dagger D_1 D_2^\dagger D_2|SU(6)\rangle, \end{aligned} \tag{4}$$

where $\vec{k}_i$ is the intrinsic three-momentum of the i parton, $k_\perp$ is the relative transverse momentum of one of the partons in the amplitude and in its complex conjugate, Ψ is the proton wave function in momentum space, and $|SU(6)\rangle$ is the spin-flavor state evaluated according to the commonly adopted $SU(6)$ symmetry. Here, as in Ref. [21], a factorization between the spin and the spatial part of the proton wave function is assumed. Let us remark that, thanks to this rigorous approach, the correct support of dPDFs is fulfilled—i.e., the dPDFs vanish in unphysical regions, i.e. $x_1 + x_2 > 1$. A proper inclusion of relativistic effects is obtained via the so-called light-front (LF) approach. This is a common procedure, largely used for the calculation of nonperturbative distributions; see e.g. Refs. [27–32]. It should be noted that dPDFs, calculated in momentum space, describe a system where two partons have a relative transverse momentum $(\pm\vec{k}_\perp)$. This unbalance physically arises since the difference of parton transverse momenta is not conserved between the amplitude and its complex conjugate [33,34]. Due to this unbalance, the dPDFs are not densities in this representation, and they cannot be interpreted as probabilistic distributions. In order to deal with distributions which admit a probabilistic interpretation, we consider the Fourier transform of Eq. (4) with respect to $\vec{k}_\perp$, which reads

$$F(x_1, x_2, \vec{b}_\perp) = \int \frac{d\vec{k}_\perp}{(2\pi)^2} e^{i\vec{k}_\perp \cdot \vec{b}_\perp} F(x_1, x_2, \vec{k}_\perp), \tag{5}$$

with $\vec{b}_\perp$ being the relative transverse distance between the two partons. In this paper, we only consider the distribution of two unpolarized quarks of flavor u (cf. Refs. [20,21,35]), so that $F(x_1, x_2, \vec{k}_\perp) \equiv F_{uu}(x_1, x_2, k_\perp)$ depends only on $k_\perp = |\vec{k}_\perp|$. Due to rotational invariance of F_{uu} in the case of unpolarized quarks, the Fourier transform reduces to

$$F(x_1, x_2, b_\perp) = \frac{1}{2\pi} \int dk_\perp k_\perp J_0(b_\perp k_\perp) F(x_1, x_2, k_\perp), \tag{6}$$

with J_0 being the Bessel function of the first kind and $b_\perp = |\vec{b}_\perp|$. Anticipating some results discussed in the next sections, we present in Fig. 1 the $b_\perp$ dependence of dPDFs at $x_1 = 0.2$, $x_2 = 0.3$. The plots show the probability of finding two partons with a given longitudinal momentum

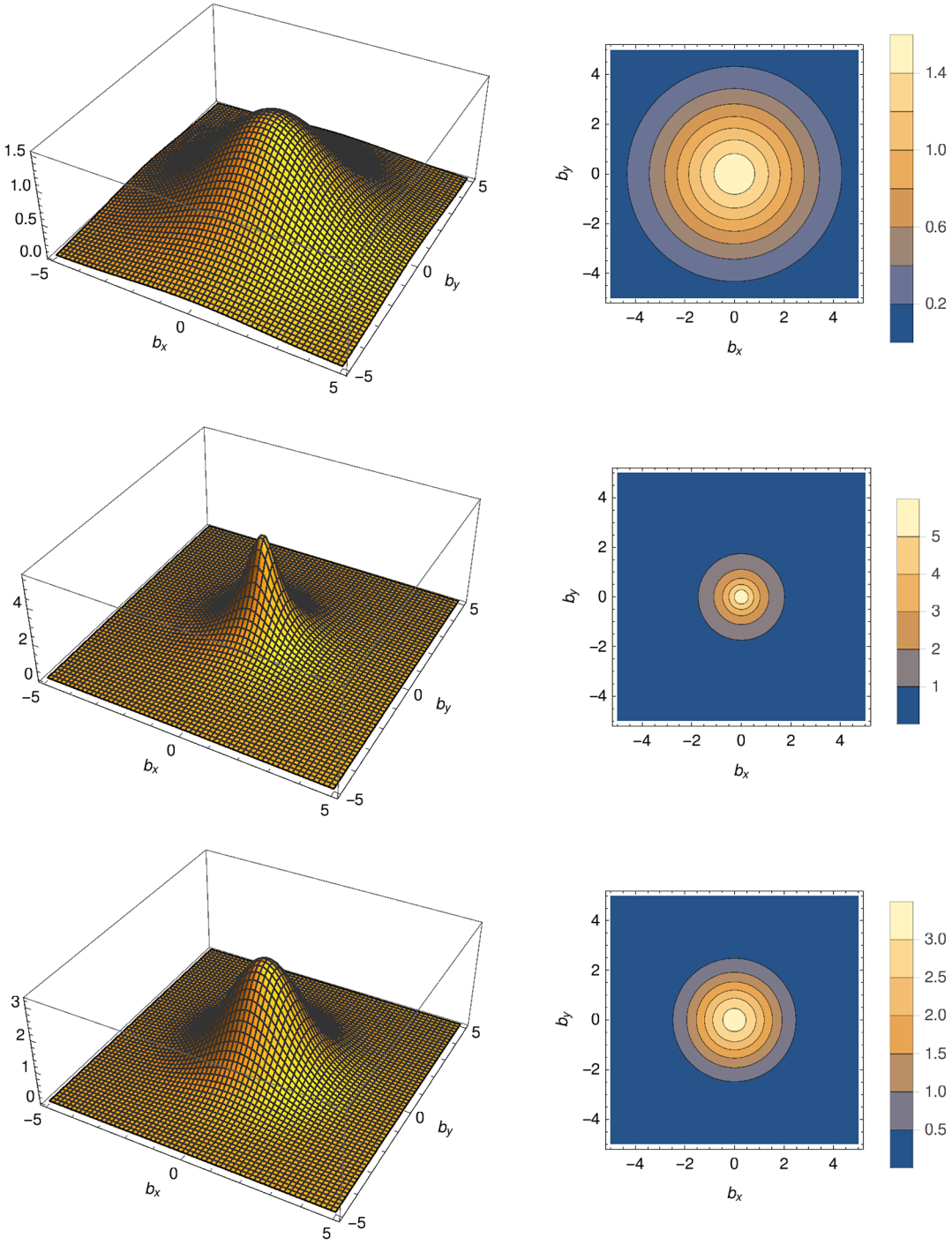

FIG. 1. Distribution evaluated via Eq. (6) by using different hadronic models presented in Sec. III—in particular, the NR (top), RL (middle), and $\mathrm{HO}_{\mathrm{rel}}$ (bottom) models at $x_1 = 0.2$, $x_2 = 0.3$.

fraction and relative transverse distance, a unique set of information which is only accessible with such distributions. The same distribution for dPDFs with longitudinal and transversally polarized quarks is likely to show departure from this symmetric structure, giving access to new details of the proton structure. These spin effects on dPDFs are presently under investigation and will be reported in a separate paper. In Eq. (4), the canonical proton wave function is calculated by means of constituent quark models (CQM). The LF proton wave function, which naturally arises in the LF approach—see e.g. Ref. [27]—is related to the canonical one thanks to the introduction of the Melosh rotations [36], which appear in the last line of Eq. (4). The latter quantities are related to LF boosts, which, in such an approach, are kinematical operators. Formally, they are defined as

$$\hat{D}_i = \frac{m + x_i M_0 + i(k_{ix}\sigma_y - k_{iy}\sigma_x)}{\sqrt{(m + x_i M_0)^2 + k_{ix}^2 + k_{iy}^2}}, \tag{7}$$

where m is the constituent quark mass; x_i is the longitudinal momentum fraction carried by the i quark; σ_x and σ_y are Pauli sigma matrices; and M_0 is the energy that the proton would have if quarks were free, and it depends on $\vec{k}_{i\perp}$ and x_i. In particular, the Melosh operators are rotations between the rest frame of the system reached through the light-front boost or canonical boost and allow us to rotate the light-front spin into the canonical one. For example, a light-front state with momentum k and spin σ, $|k,\sigma\rangle_{LF}$, can be written in terms of a canonical one, $|k,\mu\rangle_{IF}$, as follows:

$$|k,\sigma\rangle_{LF} \propto \sum_{\mu} \langle\mu|\hat{D}|\sigma\rangle |k,\mu\rangle_{IF}. \tag{8}$$

Thanks to this property, as pointed out in Ref. [27], one can convert the light-front proton wave function into the canonical one. This procedure is suitable for the calculation of nonperturbative quantities, such as parton distributions, since the proton wave function is usually evaluated by using the canonical instant form approach.

From Eq. (7), it is clear that the structure of such operators induces nontrivial correlations between the relevant variables at any energy scale. In order to visualize the effects produced by the term introduced in the last line of Eq. (4), one can analytically evaluate

$$DD^\dagger(\vec{k}_\perp, x_1, x_2, \vec{k}_{1\perp}, \vec{k}_{2\perp}) = \langle SU(6)|D_1^\dagger D_1 D_2^\dagger D_2|SU(6)\rangle. \tag{9}$$

However, since the dependence of the Melosh rotation with respect to all the variables expressed in Eq. (9) is quite complicated to visualize, we find it useful to show, as a representative case, such a dependence in the limit $DD^\dagger(\vec{k}_\perp, x_1, x_2, \vec{k}_{1\perp} = 0, \vec{k}_{2\perp} = 0)$.

For this calculation, the allowed phase space $x_1 + x_2 \leq 1$, here and in the following sections, is sampled in three different pairs of points, which we found to be representative for the effects we wish to discuss. In particular, we consider two fast partons (FF) with $x_1 = 0.2$, $x_2 = 0.3$; one slow and one fast parton (SF) with $x_1 = 0.04$, $x_2 = 0.3$; and two slow partons (SS) with $x_1 = 0.04$, $x_2 = 0.03$. The calculation of Eq. (9) with these kinematic settings is presented in Fig. 2, where one may identify three distinct regions as a function of $k_\perp$. For $k_\perp \to 0$, the Melosh operators in all kinematic configurations reduce to unity. In an intermediate region of $k_\perp$, the curves show a dip whose depth depends on the chosen kinematic configuration, and in particular, it becomes negative in the SF configuration. At larger $k_\perp$, the curves flattens out with different asymptotics. This complicated pattern, generated by the Melosh rotations, affects the calculation of dPDFs, which, in general, are distributions

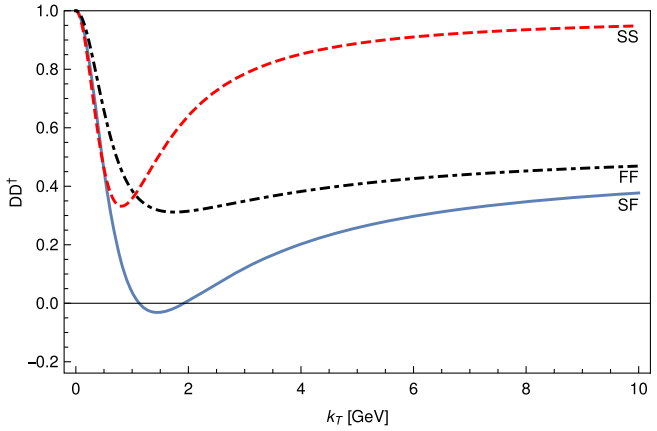

FIG. 2. The quantity Eq. (9), as a function of $k_T = k_\perp$, evaluated in different regions of x_1 and x_2, with $\vec{k}_{1\perp} = \vec{k}_{2\perp} = 0$.

evaluated also at $k_\perp \neq 0$. It is worth noting that such complicated behavior is due to the mixed combination of the four Melosh operators combined with the proton spin structure described by its wave function. Furthermore, due to the different kinematics between the proton wave function and its complex conjugate, the Melosh operators introduce kinematical breaking of the $SU(6)$ symmetry, which generates nontrivial correlations already in the unpolarized case. These kinds of effects cannot be observed in known quantities such as standard PDFs, or, e.g., in momentum distributions, given that all these distributions depend on diagonal matrix elements (i.e., evaluated at $k_\perp = 0$). In this case, in fact, the product of two Melosh operators reduces to unity. However, important effects due to the Melosh rotations can be observed in model calculations of polarized PDFs. A crucial consequence of the presence of such operators is the difference between the longitudinal and transversely polarized PDFs. In fact, since boosts commute with rotations in the nonrelativistic limit, the latter two distributions are identical in this framework—see details in Ref. [30]. Moreover, important effects are also found in the calculations of GPDs; see e.g. Refs. [27,28,30], where some distributions do not vanish due to the presence of the Melosh rotations. Conclusions along these lines are also found in the analyses of TMDs in light-front CQM calculations of Ref. [31]. Let us mention that Melosh effects can be appreciated in the calculation of nuclear spectral functions and structure functions of the ^{3}He within the light-front approach; see Refs. [37,38].

It should be noted, however, that the quantitative impact of Melosh rotations on dPDFs is weighted by the chosen proton wave function and, in particular, by its behavior at large parton momenta. We address this issue in the next section.

III. HADRONIC MODELS

The calculation of dPDFs via Eq. (4) involves, besides the relativistic boosts just described, the modeling of the (canonical) proton wave function which is obtained by

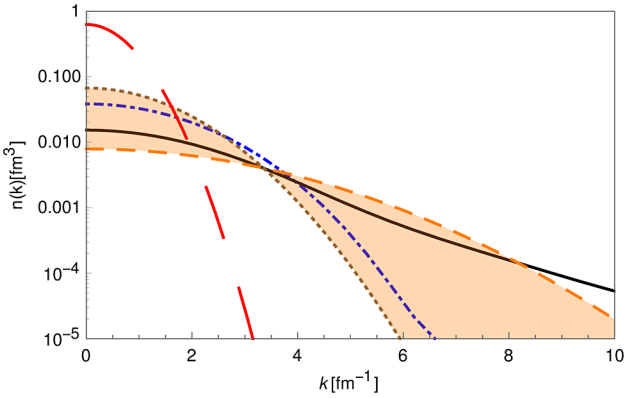

FIG. 3. Quark momentum distributions [Eq. (10)] from different models used in this analysis: RL (full black line), NR (dot-dashed blue line), original HO (dashed red line), modified HO_{nrel} (gold dotted line), and modified HO_{rel} (orange dashed line). The orange band corresponds to variation of the parameter $6 < \alpha^2 < 25$ fm^{-2}.

means of CQM. The parameters of these models are fixed by comparison with a subset of available data—e.g., the hadronic spectrum or the proton electromagnetic form factor at small momentum transfer. Since the aim of the present analysis is to identify potential model-independent effects on dPDFs, we consider a variety of proton wave functions. The first model is the so-called hypercentral quark model in both its relativistic (RL, Ref. [39]) and nonrelativistic (NR, Ref. [40]) versions. The quark momentum distributions, $n(k)$, defined in terms of the proton wave function as

$$n(k) = 3 \int d\vec{k}_1 d\vec{k}_2 \delta(\vec{k} - \vec{k}_1 - \vec{k}_2) |\Psi(\vec{k}_1, \vec{k}_2)|^2, \qquad (10)$$

are shown for the considered models in Fig. 3. The RL version (solid black) shows a broad tail extending at high momentum (hence relativistic), while the NR version (dot-dashed blue line) drops far more quickly at large momentum (hence nonrelativistic). Since both versions assume a similar potential, we also consider a modified version of the harmonic oscillator (HO); see details on the proton wave function calculated in such model in Ref. [20]. In its original version, the width of the Gaussian structure of the proton wave function is $\alpha^2 = 1.35$ fm^{-2}, where the value of the parameter is fixed by requesting that the model reproduces the slope of the proton charge form factor at zero momentum transfer. As one can see in Fig. 3, the corresponding momentum distribution (red, long dashed line) decreases rather quickly with respect to $|\vec{k}|$, the quark momentum, showing a rather extreme nonrelativistic behavior, not suitable for the estimate of relativistic effects. Given the relative mathematical simplicity of such a model, we may construct a class of models of this type by just varying the tunable parameter α in order to reproduce a momentum distribution which can have either a relativistic or nonrelativistic behavior. As shown in Fig. 3, we find that with the choice $\alpha^2 = \alpha^2_{nrel} = 6$ fm^{-2}, we can simulate a nonrelativistic model (HO_{nrel}), while with the choice $\alpha^2 = 25$ fm^{-2}, the model (HO_{rel}) develops a quite broad relativistic tail. Let us stress that for these values of the parameter α^2, the agreement between HO model predictions and available experimental data is inevitably lost. We emphasize that the behavior of the CQM models at large parton momentum determines the behavior at small x of the corresponding parton distribution functions. This feature is easily explained by considering the definition of the longitudinal momentum fraction carried by a quark in the LF approach:

$$x_1 = \frac{k_1^+}{k_1^+ + k_2^+ + k_3^+}, \qquad (11)$$

where the light-cone notation has been introduced: $a^+ = a^0 + a^3$, with a^μ being a generic four-vector. Since in Eq. (11) it is always $k^+ \geq m$, the extreme small-x region can be achieved only if e.g. $k_2^+ \gg m$—i.e., one parton has a very high momentum. Indeed, $k^+ = \sqrt{m^2 + \vec{k}^2} + |\vec{k}| \cos\theta$, with θ being the angle between the momentum vector and the z axis. Therefore, a fast drop of quark momentum distributions at large $|\vec{k}|$—that is, a nonrelativistic behavior, determines a smooth vanishing of PDFs as $x \to 0$. On the contrary, PDFs corresponding to relativistic models still vanish in the limit $x \to 0$, but with a much harder behavior. All these results are summarized in Fig. 4, where the u-quark distributions, obtained from all the considered models, are compared together. With this selection of models, based on different potentials and showing different relativistic behavior, we now turn to the evaluation and discussion of dPDFs.

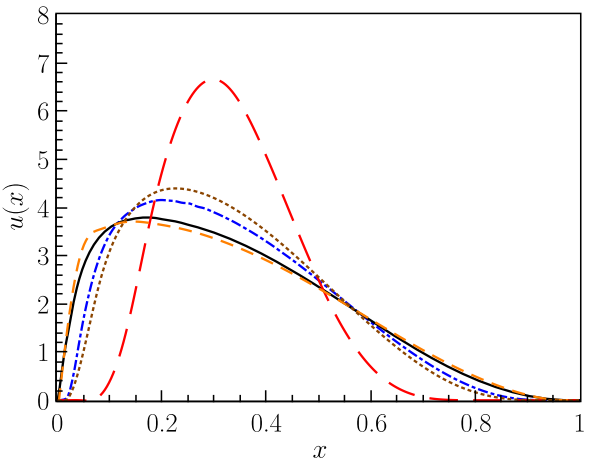

FIG. 4. Single-parton distributions calculated with the different models used in this analysis: RL (full black line), NR (dot-dashed blue line), original HO (dashed red line), modified HO_{nrel} (gold dotted line), and modified HO_{rel} (orange dashed line).

IV. CALCULATIONS OF dPDFs

A. Breaking the factorized ansatz

As already mentioned in the previous sections, to date, the experimental knowledge on the DPS cross section is limited to inclusive observables extracted by using Eqs. (1) and (3), and the corresponding assumptions. It is therefore clear that investigating dPDF modelization beyond the assumptions in Eq. (2) will require more differential DPS measurements. In order to fill this lack of knowledge, a fully factorized form for dPDFs in all the relevant variables, as indicated in Eq. (2), is often assumed, which aims to maximally exploit the current knowledge on the proton structure.

On the other hand, in the moderate large values of fractional momenta, x, natural domain of CQM with realistic potentials, as discussed in Refs. [20,21,35], calculations show that both the factorization of dPDFs as a product of single-parton distributions and, perhaps more interestingly, the $(x_1, x_2) - k_\perp$ factorization are violated. For recent results on the breaking of the factorization on the x_1 and x_2 dependence, see Ref. [41]. Furthermore, the breaking of the $(x_1, x_2) - k_\perp$ factorization might be generated both by the specific form of the proton wave function and by relativistic effects induced by Melosh operators.

The purpose of this section is to investigate in more detail the latter effect. Within this context, the harmonic oscillator model appears to be particularly suitable to quantify to what extent such factorization breaking is due to relativistic effects alone. Within this model, in fact, the $(x_1, x_2) - k_\perp$ dependences are entirely factorized; see Ref. [20]. In order to estimate these effects quantitatively, we evaluate the ratio

$$R_N(x_1, x_2, b_\perp) = \frac{F(x_1, x_2, b_\perp)}{\int d\vec{b}_\perp F(x_1, x_2, b_\perp)}. \qquad (12)$$

It is worth noting that, according to Eq. (5), $\int d\vec{b}_\perp F(x_1, x_2, b_\perp) = F(x_1, x_2, k_\perp = 0)$, so the denominator in Eq. (12) does not depend on the Melosh rotations which reduce to unity in the $k_\perp \to 0$ limit; see Fig. 2. The ratio given in Eq. (12), calculated by using $\mathrm{HO_{rel}}$, is presented in Fig. 5. The ratio R_N with dPDFs evaluated without the Melosh rotations gives identical (superimposed) results in the three kinematic regions of x_1 and x_2, as expected. On the contrary, if Melosh rotations are taken into account, we observe a significant reduction of the magnitude of dDPFs and a progressive broadening of the $b_\perp$ dependence with respect to the distribution without Melosh, depending on the partonal fractional momenta x_i. This effect is sizeable, especially in the SF configuration. This observation leads us to conclude that for dPDFs evaluated through models [which themselves may or may not show a $(x_1, x_2) - k_\perp$ factorization] via Eq. (4), at the hadronic scale, relativistic effects induce significant factorization-breaking effects. This result suggests that future model building of dPDFs may take into account the possibility of modulating the dPDFs $b_\perp$ dependence as a function of parton fractional momenta.

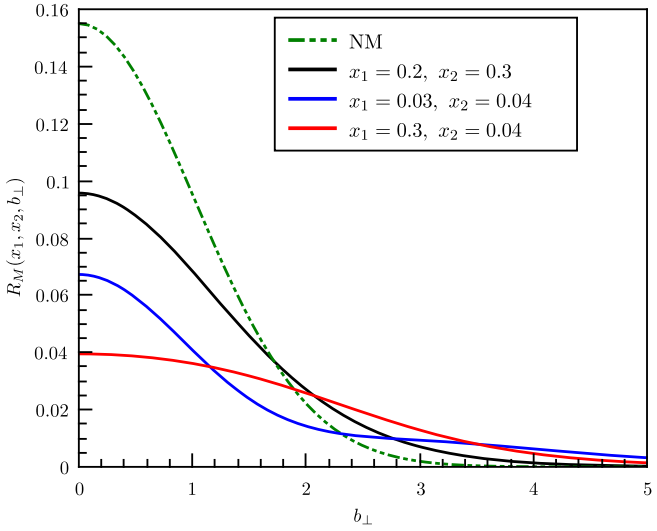

FIG. 5. The ratio (12) evaluated using the $\mathrm{HO_{rel}}$ model in three different regions of x_1 and x_2 as a function of $b_\perp = |\vec{b}_\perp|$. In the legend, the acronym "NM" specifies the calculation in which the Melosh rotations are neglected.

B. Relativistic effects

It appears from the previous section that Melosh rotations do not allow us, in general, to factorize dPDFs in longitudinal and transverse distributions. More importantly, they cause a significant reduction of the distributions, which, in turn, induces substantial variation of the corresponding DPS cross section. In order to further investigate these effects, in this section we calculate dPDFs in $b_\perp$ space via Eq. (6) with and without Melosh rotations. We note that in the latter case, we basically reduce to the results presented in Refs. [19–21]. The results of these calculations are shown in Fig. 6, where predictions from different models are presented in columns and different kinematical configurations in rows. The $b_\perp$ spectra without Melosh rotation (NM) show a great variety in magnitude and width, reflecting the differences in the used proton wave functions. In all cases, the distributions are peaked at $b_\perp = 0$ and show a finite behavior in the short-distance limit. If Melosh rotations are included (red dotted lines), we observe a significant reduction of the magnitude of the distributions. In particular, in the SF kinematics, the magnitude of the suppression is more pronounced, and for the RL models (left panel, middle row), the distribution tends to decrease as $b_\perp \to 0$, and it does show a maximum shifted to a nonvanishing value of $b_\perp$. We conclude that for relativistic models, in the SF region, these operators discourage the partons from being close to each other. This model-dependent behavior results from the combined effect

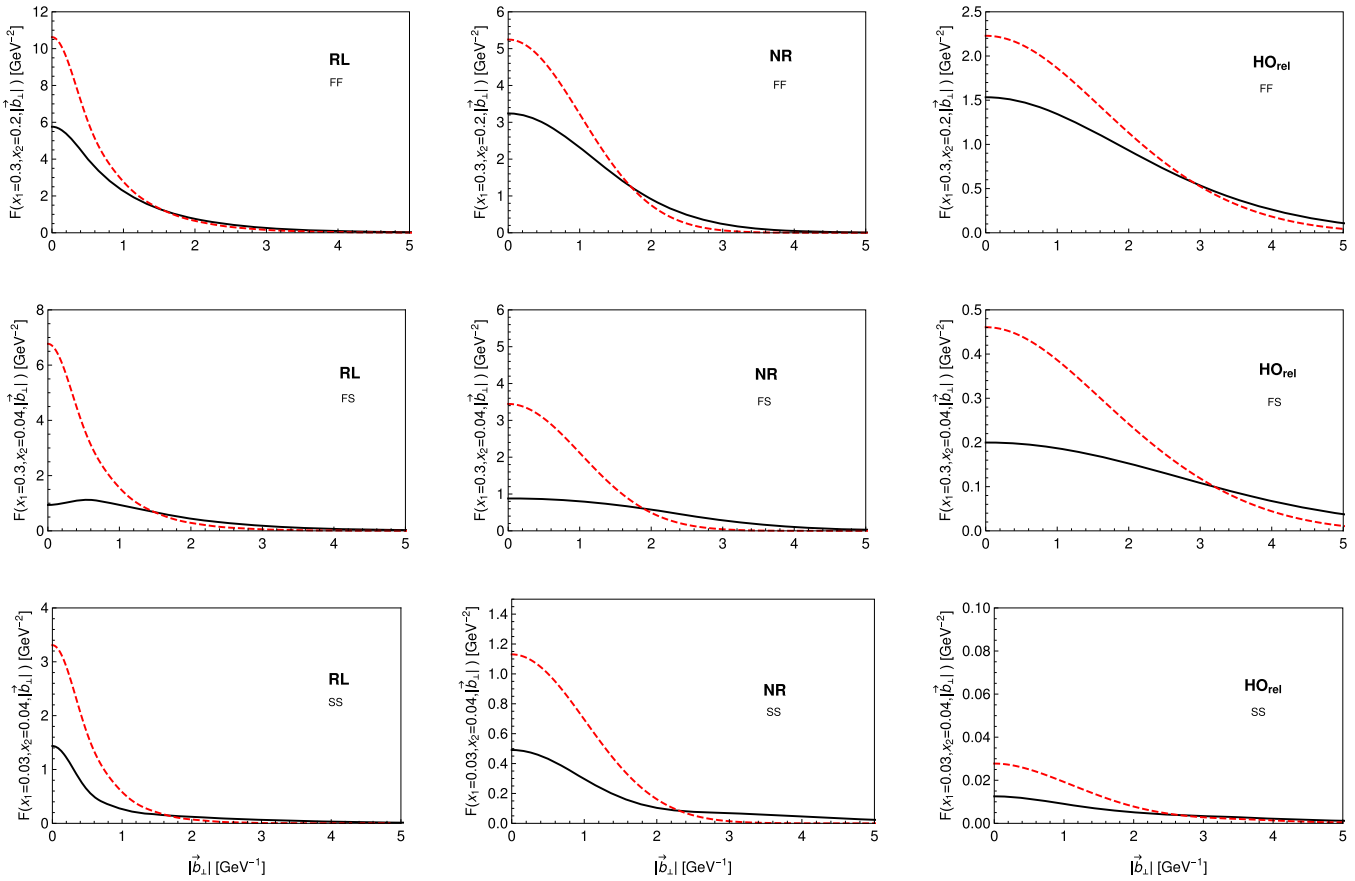

FIG. 6. The distribution Eq. (6) as a function of $|\vec{b}_\perp|$ evaluated in three different kinematical configurations (from top to bottom, FF, SF, and SS) using the relativistic model, the NR one and the $\mathrm{HO_{rel}}$ one (from left to right). Lines correspond to the evaluation of Eq. (6) with (black) and without (red) the Melosh rotations.

of the negative contributions of the Melosh rotations in Eq. (6) and the large $|\vec{k}|$ tail of the RL model. The amount of the suppression, induced by the Melosh operators, is again conveniently quantified by studying the ratio

$$R(x_1, x_2, \vec{b}_\perp) = \frac{F(x_1, x_2, b_\perp)}{F_{NM}(x_1, x_2, b_\perp)}, \tag{13}$$

where $F_{NM}(x_1, x_2, b_\perp)$ is the distribution in Eq. (4) once the Melosh rotations are neglected. The corresponding results are reported in Fig. 7, where it is shown that the suppression slightly depends on the kinematical configurations, being smaller in the FF case, and on average, around 0.5 in the FS and SS regions. Moreover, such suppression is rather model independent, as can be inferred by the relatively contained spread of the orange band. In all the previous sections, the

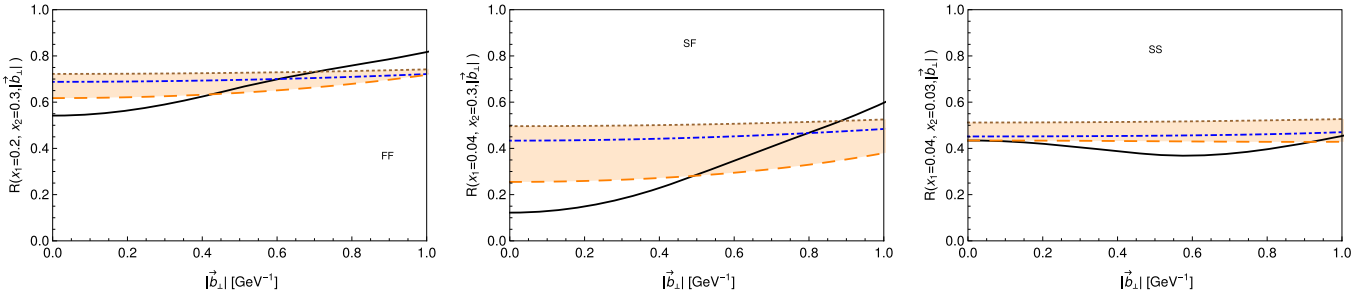

FIG. 7. The ratio in Eq. (13) evaluated as a function of $|b_\perp|$ in different kinematic regions: $x_1 = 0.2$, $x_2 = 0.3$ (left panel); $x_1 = 0.04$, $x_2 = 0.3$ (middle panel); and $x_1 = 0.04$, $x_2 = 0.03$ (right panel): RL (full black line), NR (dot-dashed blue line), original HO (dashed red line), modified $\mathrm{HO_{nrel}}$ (gold dotted line), and modified $\mathrm{HO_{rel}}$ (orange dashed line). The orange band corresponds to variation of the parameter $6 < \alpha^2 < 25$ fm^{-2}.

main effects of the Melosh rotations have been analyzed directly on the dPDFs, either in momentum or in coordinate space. It is worth remarking, however, that dPDFs appear in the DPS cross section in a convolution-like formula which reads [1]

$$\sigma_{\mathrm{DPS}}^{A+B} \propto \sum_{abcd} \int d\vec{b}_\perp F_{ac}(b_\perp) F_{cd}(b_\perp) \hat{\sigma}_{ab}^{A} \hat{\sigma}_{cd}^{B}, \quad (14)$$

where we have suppressed the dependences on longitudinal fractional momenta, and $\hat{\sigma}$ are the elementary partonic cross sections for the process $ab(cd) \to A(B)X$. It is therefore clear that the details of the $b_\perp$ dependence of the dPDFs get obscured by the convolution, and it is intertwined with the dependences on longitudinal fractional momenta. In this respect, we notice that a more direct access to the transverse structure of dPDFs may be provided by analyzing the DPS component in multijet photoproduction in ep or pp collisions. In this case, the quasireal photon, emitted either by the electron or the proton and fluctuating in $q\bar{q}$ dipoles, probes the parton pair in the nucleon at a relative transverse distance of the order $b_\perp \sim 1/Q$ [42–44], while its low virtuality Q can be controlled experimentally. In the present context, a proper calculation of σ_{eff} via Eq. (14) requires the selection of a definite final state $A + B$, the evaluation of corresponding partonic cross sections, and the perturbative evolution of dPDFs from the hadronic scale (in the present work $\mu_0 = 0.1$ GeV^2, where only three valence quarks carry the proton momentum) to the scales μ_A and μ_B characterizing the hard processes. We will report on these results in a separate publication. In the present work, in order to get a quantitative estimate of the possible role of the Melosh on observable-related quantities, following the lines of Refs. [25,26], we define the ratio

$$R_\sigma(x_1, x_2) = \frac{\int d\vec{b}_\perp F_{NM}(x_1, x_2, b_\perp)^2}{\int d\vec{b}_\perp F(x_1, x_2, b_\perp)^2}, \quad (15)$$

where the square is taken to mimic the analytic structure of the DPS cross section in Eqs. (14) and (3). The ratio in Eq. (15) has been calculated by using the addressed models in the three kinematics configurations. The results are presented in Table I. One should notice that in regions where the three CQMs are completely different, the effects of the Melosh are rather independent on the choice of the detailed proton structure considered. For the sake of transparency, some

TABLE I. The ratio $R_\sigma(x_1, x_2)$ calculated for different kinematical configurations and adopted models.

	RL	NR	$\mathrm{HO_{rel}}$	$\mathrm{HO_{nrel}}$
$R_\sigma(x_1 = 0.03, x_2 = 0.04)$	4.83	2.80	4.12	2.36
$R_\sigma(x_1 = 0.04, x_2 = 0.3)$	4.33	2.27	3.66	2.05
$R_\sigma(x_1 = 0.2, x_2 = 0.3)$	1.85	1.50	1.73	1.73

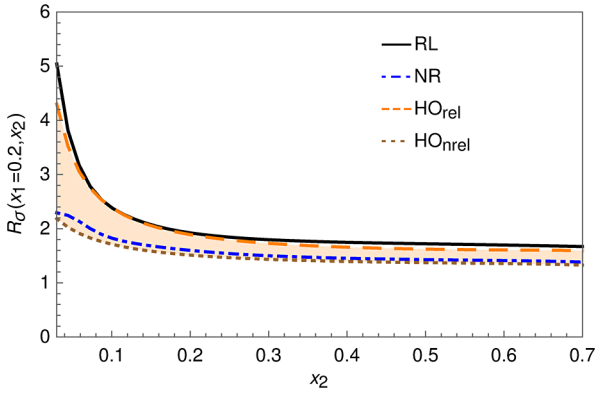

FIG. 8. The ratio $R_\sigma(x_1, x_2)$ calculated for fixed values x_1 as a function of x_2 within all the adopted models.

differences are found when small x are involved in the calculation. This feature can be seen as a limit of the present analysis. In fact, as already mentioned, the low-x region is associated with high momenta, where the three CQMs substantially differ from each other, and details of the models cannot be totally separated by those of the relativistic treatment. As shown in Fig. 8, the spread of R_σ calculated within different models increases for decreasing x_2. This reflects different modelizations of the proton wave function at high quark momenta; see Fig. 4. Nevertheless, it should be noted that the value of the ratio and its spread, induced by different models, become constant for approximately $x_2 > 0.1$. Therefore, we may conclude that, in the valence region, the suppression factor (a factor around 2) induced by Melosh rotations is quite a model-independent effect.

V. CONCLUSIONS

In this work, we have presented a quantitative analysis of relativistic effects on dPDFs. This analysis has been provided thanks to the correct treatment of dPDF in a relativistic framework due to the LF approach, which implies the introduction of the so-called Melosh rotations in order to achieve a full Poincarè covariant description of dPDFs. We have discussed to what extent the Melosh rotations alone may affect the often assumed factorization in $(x_1, x_2) - k_\perp$ space, which is commonly adopted in experimental analyses to extract the DPS cross section. We have found that once relativistic effects are included, the dPDFs spectrum in $b_\perp$ space does depend on the parton fractional momenta, an effect beyond the assumptions in Eq. (2). For example, for relativistic models in the low-x region with a large unbalance of longitudinal momenta, relativistic effects prevent the two partons from being close to each other in transverse space.

Furthermore, we have found that the main effect of the relativistic treatment is to produce a strong reduction of the size of the dPDFs with respect to the same calculation where such operators are omitted. By employing appropriate ratios, we have shown that these results only mildly

depend on the assumed proton wave function and that such a suppression ranges from a factor of 2 in the FF configuration to 4 in the SS one. On general grounds, we may expect that the perturbative evolution of dPDFs, performed at a fixed value of $b_\perp$, will propagate these correlations, found at low-scale and moderate values of x, to higher scales and lower values of x. However, their quantitative impact on observables can be only properly assessed with dedicated analyses of selected DPS processes. In closing, we have found that relativistic effects on dPDFs are sizeable and that they should be always taken into account in these kinds of model calculations.

ACKNOWLEDGMENTS

This work is supported in part through the project "Hadron Physics at the LHC: Looking for signatures of multiple parton interactions and quark gluon plasma formation (Gossip project)," funded by the "Fondo ricerca di base di Ateneo" of the Perugia University. This work was supported in part by the Mineco under Contracts No. FPA2013-47443-C2-1-P and No. SEV-2014-0398. We warmly thank Sergio Scopetta, Vicente Vento, Marco Traini, Jonathan Gaunt, and Alberto Accardi for many useful discussions.

[1] N. Paver and D. Treleani, Nuovo Cimento A **70**, 215 (1982).
[2] M. Mekhfi, Phys. Rev. D **32**, 2371 (1985).
[3] T. Sjostrand and M. Van Zijl, Nuovo Cimento A **70**, 215 (1982).
[4] G. Calucci and D. Treleani, Phys. Rev. D **60**, 054023 (1999).
[5] J. R. Gaunt and W. J. Stirling, J. High Energy Phys. 03 (2010) 005.
[6] F. A. Ceccopieri, Phys. Lett. B **734**, 79 (2014).
[7] M. Diehl and A. Schafer, Phys. Lett. B **698**, 389 (2011).
[8] M. Diehl, D. Ostermeier, and A. Schafer, J. High Energy Phys. 03 (2012) 089.
[9] A. M. Snigirev, Phys. Rev. D **68**, 114012 (2003).
[10] F. A. Ceccopieri, Phys. Lett. B **697**, 482 (2011).
[11] H. Jung *et al.*, *Proceedings, 7th International Workshop on Multiple Partonic Interactions at the LHC* (MPI@LHC, 2015), https://bib-pubdb1.desy.de/record/297386.
[12] T. Akesson *et al.* (Axial Field Spectrometer Collaboration), Z. Phys. C **34**, 163 (1987).
[13] J. Alitti *et al.* (UA2 Collaboration), Phys. Lett. B **268**, 145 (1991).
[14] F. Abe *et al.* (CDF Collaboration), Phys. Rev. D **56**, 3811 (1997).
[15] V. M. Abazov *et al.* (D0 Collaboration), Phys. Rev. D **81**, 052012 (2010).
[16] G. Aad *et al.* (ATLAS Collaboration), New J. Phys. **15**, 033038 (2013).
[17] S. Chatrchyan *et al.* (CMS Collaboration), J. High Energy Phys. 03 (2014) 032.
[18] R. Aaij *et al.* (LHCb Collaboration), J. High Energy Phys. 04 (2014) 091.
[19] H. M. Chang, A. V. Manohar, and W. J. Waalewijn, Phys. Rev. D **87**, 034009 (2013).
[20] M. Rinaldi, S. Scopetta, and V. Vento, Phys. Rev. D **87**, 114021 (2013).
[21] M. Rinaldi, S. Scopetta, M. Traini, and V. Vento, J. High Energy Phys. 12 (2014) 028.
[22] W. Broniowski and E. Ruiz Arriola, Few-Body Syst. **55**, 381 (2014).
[23] W. Broniowski, E. Ruiz Arriola, and K. Golec-Biernat, Few-Body Syst. **57**, 405 (2016).
[24] T. Kasemets and A. Mukherjee, Phys. Rev. D **94**, 074029 (2016).
[25] M. Rinaldi, S. Scopetta, M. Traini, and V. Vento, Phys. Lett. B **752**, 40 (2016).
[26] M. Traini, S. Scopetta, M. Rinaldi, and V. Vento, arXiv: 1609.07242.
[27] S. Boffi, B. Pasquini, and M. Traini, Nucl. Phys. **B649**, 243 (2003).
[28] S. Boffi, B. Pasquini, and M. Traini, Nucl. Phys. **B680**, 147 (2004).
[29] B. Pasquini, M. Traini, and S. Boffi, Phys. Rev. D **71**, 034022 (2005).
[30] B. Pasquini, M. Pincetti, and S. Boffi, Phys. Rev. D **72**, 094029 (2005).
[31] B. Pasquini, S. Cazzaniga, and S. Boffi, Phys. Rev. D **78**, 034025 (2008).
[32] M. Traini, Phys. Rev. D **89**, 034021 (2014).
[33] B. Blok, Y. Dokshitser, L. Frankfurt, and M. Strikman, Eur. Phys. J. C **72**, 1963 (2012).
[34] B. Blok, Y. Dokshitzer, L. Frankfurt, and M. Strikman, Eur. Phys. J. C **74**, 2926 (2014).
[35] A. V. Manohar and W. J. Waalewijn, Phys. Rev. D **85**, 114009 (2012).
[36] H. J. Melosh, Phys. Rev. D **9**, 1095 (1974).
[37] A. Del Dotto, E. Pace, G. Salmé, and S. Scopetta, Phys. Rev. C **95**, 014001 (2017).
[38] E. Pace, G. Salme, S. Scopetta, A. Del Dotto, and M. Rinaldi, Few-Body Syst. **54**, 1079 (2013).
[39] P. Faccioli, M. Traini, and V. Vento, Nucl. Phys. **A656**, 400 (1999).
[40] M. Ferraris, M. M. Giannini, M. Pizzo, E. Santopinto, and L. Tiator, Phys. Lett. B **364**, 231 (1995).
[41] M. Rinaldi, S. Scopetta, M. C. Traini, and V. Vento, J. High Energy Phys. 10 (2016) 063.
[42] B. Blok and M. Strikman, Eur. Phys. J. C **74**, 3214 (2014).
[43] J. M. Butterworth, J. R. Forshaw, and M. H. Seymour, Z. Phys. C **72**, 637 (1996).
[44] J. R. Gaunt, J. High Energy Phys. 01 (2013) 042.